Theoretical and Experimental Investigation of Morphology and Temperature Effects on Adsorption of Organic Vapors in Single-Walled Carbon Nanotubes

Sandeep Agnihotri,*,† José P. B. Mota,*,‡ Massoud Rostam-Abadi,§ and Mark J. Rood⊥

Department of Civil and Environmental Engineering, University of Tennessee, Knoxville, Tennessee 37996-2010, Requimte/CQFB, Departamento de Quimica, Faculdade de Ciencias e Tecnologia, Universidade Nova de Lisboa, 2829-516 Caparica, Portugal, Illinois State Geological Survey, 615 East Peabody Drive, Champaign, Illinois 61820, and Department of Civil and Environmental Engineering, University of Illinois, Urbana−Champaign, 205 North Mathews Avenue, Urbana, Illinois 61801

Received: January 3, 2006; In Final Form: February 20, 2006

Hexane adsorption on single-walled carbon nanotube (SWNT) bundles is studied by both simulation and experimentally using a previously developed computer-aided methodology, which employed a smaller physisorbed probe molecule, nitrogen, to explore the porosity of nanotube samples. Configurational-bias grand canonical Monte Carlo simulation of hexane adsorption on localized sites of the bundles is carried out to predict adsorption on their external surface and in their internal sites. These localized isotherms are then combined into a global isotherm for a given sample by using knowledge of its tube-diameter distribution and structural parameters, such as the fraction of open-ended nanotubes and the external surface area of bundles in samples, which have been independently determined from the standard nitrogen adsorption isotherm. The near-perfect replication of experimental isotherms demonstrates the validity of our method for structural characterization of SWNT samples. The effect of temperature on adsorption is also studied and the simulation results are extrapolated to predict the limiting hexane adsorption capacity of the samples. The similarity between the hexane adsorption isotherms and those of other organic molecules demonstrates that the adsorption mechanisms explored here are not specific to hexane, and that the proposed methodology can be potentially applicable to other sorbates with equal success.

1. Introduction

The unique one-dimensional nanometric structure of single-walled carbon nanotubes (SWNTs) imparts remarkable properties[1] because of which various potential applications have been suggested.[2] The hollow nanoscaled structure of SWNTs is especially attractive for their use as membranes, adsorbents, catalyst supports, and related materials.[2] These applications may be realized by availability of more detailed information on the porosity and adsorption mechanisms of these materials.

Adsorption properties of a nanotube sample depend on three factors, the first of which is the contribution of individual adsorption sites (Figure 1). Due to strong van der Waals interaction, SWNTs adhere to each other and form bundles. The adsorption sites, therefore, are defined for a bundle and not an individual nanotube.[3−5] Adsorption can occur inside nanotubes (endohedral sites), in the interstitial channels between nanotubes, in the outer grooves present on the peripheral surface of the bundles where two nanotubes meet, and on the remaining peripheral surface of the bundles. The adsorption capacity and mechanism of individual sites are unique, which may be affected by surface functionality and structural deformations.[6]

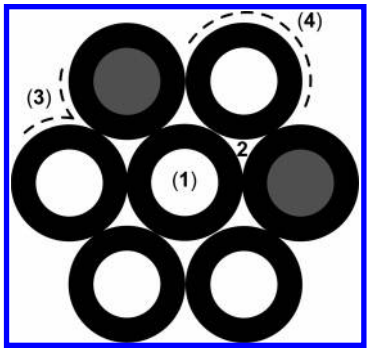

Figure 1. Different adsorption sites on a homogeneous bundle of partially open-ended SWNTs: (1) internal, (2) interstitial channel, (3) external groove site, and (4) external surface.

Second, the fraction of nanotubes that are opened and unblocked can greatly influence the overall adsorption capacity of a sample.[7] Their internal pore volume, where the majority of adsorption capacity resides, is accessible. Close-ended nanotubes, or those whose tips are blocked by surface functional groups, however, contribute little toward total adsorption, as adsorption occurs only in the interstitial channels and on the external surface of the bundle. Therefore, common analytical methods used to measure the adsorption capacity of a sample (such as gravimetric analysis) underestimate the limiting adsorption capacity of the sample because close-ended or blocked nanotubes do not contribute to the microporosity of the sample. Subjecting nanotube samples to a heat treatment is one approach to open more nanotubes.[8]

* Address correspondence to these authors.
† University of Tennessee. Phone: (865) 974-7728. Fax (865) 974-7699. E-mail: sagnihot@utk.edu.
‡ Universidade Nova de Lisboa. Phone: (351) 212948300. Fax: (351) 212948385. E-mail: pmota@dq.fct.unl.pt.
§ Illinois State Geological Survey. Phone: (217) 244-4977. Fax: (217) 333-8566. E-mail: massoud@isgs.uiuc.edu.
⊥ University of Illinois. Phone: (217) 333-6963. Fax: (217) 333-6968. E-mail: mrood@uiuc.edu.

10.1021/jp060040a CCC: $30.25
Published on Web 03/24/2006

Third, the purity of a sample can be a limitation in itself. This is because nanotubes are often found mixed with impurities, such as carbon coated catalyst particles, soot, and other forms of carbons, which can be adsorbent materials on their own, and avoiding their presence can grossly misrepresent adsorption properties of nanotubes. The adsorptive contribution of impurities in nanotube samples is still largely unexplored.

Significant progress has been made on exploiting the adsorption properties of nanotubes. It has been reported that adsorption surface area and porosity of nanotubes continues to evolve for several months after their manufacture.[6] The use of nanotubes as nanoscaled cylinders for trapping small adsorbate molecules is being actively explored.[9] Furthermore, it is now known that adsorbed molecules can alter the electrical properties of nanotubes,[10,11] which can be used for developing sensors.[12,13] The high adsorption capacity, which is predicted by simulation for narrow nanotubes that are separated by large interstitial spacing,[14] is yet to be achieved experimentally by using molecular spacers. Other significant studies have revealed that nanotubes are good and reversible adsorbents for NO from flue gases,[15] Ar can be trapped inside nanotubes at pressures as high as 60 MPa,[16] mechanisms of Kr adsorption in nanotubes are similar to those on graphite,[17] two distinct adsorption surfaces are present on SWNTs,[18] capillary condensation occurs at subcritical temperatures inside open nanotubes,[19] and whether gases actually adsorb in the interstitial channels of SWNT bundles.[5,20]

Despite considerable effort, the interaction between organic molecules and nanotubes remains largely unexplored. The limited number of theoretical and experimental studies has focused on adsorption of small molecules on carbon nanotubes. Theoretical studies have explored interactions of small organic molecules, such as CH_4, with nanotubes[20−22] and have reported mechanisms for separation of binary mixtures of simple alkanes by diffusive flow through carbon nanotubes.[22] A few experimental studies have described adsorption isotherms for benzene, methanol,[23] and methane,[3] high affinity of nanotubes for ppb levels of dioxins,[24] adsorption kinetics of ethanol, 2-propanol, cyclohexane, benzene, and hexane on SWNTs,[25] direct applicability of nanotubes as adsorbent traps for volatile organic compounds,[26,27] and adsorption capacities for hazardous organic air pollutants.[28]

In this study, the adsorption mechanism and capacity of organic molecules on SWNT bundles are investigated by molecular simulation and experimentally. Hexane was selected as a model organic adsorbate. To determine its adsorption on localized sites of SWNT bundles, a series of configurational-bias grand canonical Monte Carlo simulations are performed, whose results are directly compared with adsorption measurements at various temperatures.[28] The simulation procedure was developed as part of our previous research on computer-aided analysis of SWNT bundles,[7] where sample morphology is combined with molecular simulation and physisorption experiments with use of a small probe molecule for determining structural parameters fundamental to adsorption in SWNTs: specific external surface area of the bundles and fraction of open-ended SWNTs.

Here, we demonstrate that the same simulation methodology and the structural parameters obtained earlier can be applied to accurately predict the adsorption of larger, more complex organic molecules. Near perfect replication of experimental hexane isotherms is obtained by simulation over a wide temperature range. This establishes the validity and versatility of the simulation procedure developed earlier.[7] In particular, it shows that the values of specific external surface area of the sample and fraction of accessible endohedral and interstitial sites determined by probing the porosity of the sample with physisorbed N_2 remain unchanged for adsorption of a larger, flexible chain molecule such as hexane. Structural parameters depend on nanotube geometry and should be independent of the methodology and physical properties of the sorbate molecule used, as long as it is sufficiently small for probing the microporosity of the sample to the full extent; this is what is demonstrated here.

TABLE 1: Purity and Morphology of SWNT Samples

	wt %[a]			
sample	SWNTs	impurities	diameter, D (Å)[b]	wt fraction, w_D[b]
EA95	≈95	≈5	11.5	0.15
			14.0	0.34
			15.2	0.51
CVD80	≈80	≈20	9.0	0.42
			10.2	0.21
			10.7	0.17
			11.1	0.11
			11.8	0.10

[a] Manufacturer specified information. [b] Determined by Raman analysis.

The molecular simulation study of hexane adsorption on localized sites of SWNT bundles at various temperatures shows that the experimentally observed lowering of its adsorption capacity with increasing temperature is primarily due to decreased adsorption on the external surface of the bundles and not inside the nanotubes. We have also calculated the limiting hexane adsorption capacity for each sample and predicted isotherms for a hypothetical scenario where all nanotubes are opened and unblocked. Additionally, it is found that simulated hexane isotherms follow the same trend as those of other organic compounds, which shows that the adsorption mechanisms explored in this study are likely to be of general applicability to most organic vapors on SWNTs.

2. Experiments, Simulation, and Analytical Methods

Molecular simulations were carried out to predict hexane adsorption on two commercially available purified samples of SWNT bundles. Sample description and characterization details are available elsewhere[6] and only a brief description of those results is presented here for clarity. The selected samples were synthesized by two methods: electric-arc and HiPco chemical vapor deposition (CVD),[29,30] to provide different SWNT morphology and contamination levels. Both samples were produced by the manufacturer from purification of as-grown nanotubes. The electric-arc sample (EA95) contains 95−98 wt % SWNTs, whereas the HiPco CVD sample (CVD80) is slightly more impure (≈80 wt % nanotubes). The nanotube-diameter distribution of each sample was determined by Raman analysis and converted to a discrete histogram (Table 1) by selecting the larger peaks of the radial breathing frequency. The majority of SWNTs present in sample EA95 are 15.2 Å in diameter and those in sample CVD80 are 9 Å wide.

Hexane adsorption isotherms on samples EA95 and CVD80 were determined gravimetrically in an earlier study, the details of which can be found elsewhere.[28] The isotherms were measured at 298.15, 310.15, and 323.15 K, for relative vapor pressures ranging from 10^{-4} to $0.9P/P_0$, where P is the actual vapor pressure and P_0 is the saturation vapor pressure at the particular temperature. The samples exhibited "aging", that is their nitrogen BET surface areas and pore volumes changed over a period of several months from the time when the sample

TABLE 2: Lennard-Jones Potential Parameters

pseudoatom	ϵ/k_B (K)	σ (Å)
C (SWNT)	28	3.40
CH_3	98	3.75
CH_2	46	3.95

was manufactured.[6] Therefore, the organic vapor adsorption study was performed after "aging" had stabilized (7 months < sample age < 16 months).

The molecular simulations were carried out to model experimental conditions. The computational procedure was developed previously to simulate nitrogen adsorption at its normal boiling point (77 K) on the same samples. A detailed discussion of the method can be found elsewhere.[7] A brief description of adsorbent model and computational method are given below, with emphasis on its extension to efficiently handle flexible chain molecules such as hexane.

The hexane molecule is considered as a flexible chain of pseudoatoms. The interaction between the carbon atoms of a nanotube and each site of the hexane molecule is modeled by using the Lennard-Jones potential

$$u_{ij}(r) = 4\epsilon_{ij}[(\sigma_{ij}/r)^{12} - (\sigma_{ij}/r)^{6}] \quad (1)$$

as is the nonbonded interaction between the sites on different hexane molecules or sites within a hexane molecule that are separated by more than three bonds. In eq 1, r is the intermolecular distance; the well depths, ϵ_i/k_B, where k_B is the Boltzmann constant, and collision diameters, σ_i, used are given in Table 2. The cross terms were obtained by using the standard Lorenz−Berthelot combining rules: $\epsilon_{ij} = (\epsilon_i\epsilon_j)^{1/2}$ and $\sigma_{ij} = (\sigma_i + \sigma_j)/2$.

The force field adopted for hexane is the transferable potential for phase equilibria (TraPPE),[31] which is based on a united-atom model where each CH_3 or CH_2 group is treated as a single interaction site. Adjacent pseudoatoms of a hexane molecule are connected by a rigid bond length of 1.54 Å; the harmonic bond-bending potential $U_{bend}(\theta)$, along three successive pseudoatoms, is governed by

$$U_{bend} = k_\theta(\theta - \theta_0)^2/2 \quad (2)$$

with force constant $k_\theta/k_B = 62500$ K rad^{-2} and equilibrium bending angle $\theta_0 = 114°$. The dihedral torsion potential $U_{tors}(\phi)$, along four successive pseudoatoms, is modeled by using

$$U_{tors} = c_1[1 + \cos\phi] + c_2[1 - \cos(2\phi)] + c_3[1 + \cos(3\phi)] \quad (3)$$

with $c_1/k_B = 355.03$ K, $c_2/k_B = -68.19$ K, and $c_3/k_B = 791.32$ K.

Each SWNT in the bundle is considered to be a smooth, structureless nanocylinder of infinite length, for which an effective potential is developed by numerically integrating the C-pseudoatom potential over the positions of all carbon atoms in the tube. To speedup the calculations, the solid−fluid potential is pretabulated and reconstructed during the simulations, using cubic Hermite polynomial interpolation. Each bundle was constructed by assembling various SWNTs in the usual periodic hexagonal arrangement (Figure 1), with the van der Waals gap between nanotubes fixed at 3.4 Å.

Attempts to apply the normal GCMC technique to large sorbates or to systems in which the sorbates fit very tightly into the pores result in very low acceptance rates of the insertion and deletion steps needed to sample the grand canonical ensemble correctly. Furthermore, not all portions of the accessible pore space of the bundle are equally favorable; there exist preferred regions in which sorbate molecules are localized. This information can be incorporated into a GCMC simulation if insertions are not attempted randomly throughout the volume, but rather are performed such that sorbates are inserted preferentially into the most favorable locations of the pore space of the bundle. This provides a substantial improvement in the efficiency of the simulation compared to traditional GCMC.

To enhance the sampling of configurational space and increase the acceptance rate of the particle insertion/removal step, we resort to configurational-bias sampling techniques.[32−34] In the configurational-bias GCMC method a molecule is grown atom-by-atom trying not to overlap with the other atoms. For the placement of the first CH_3 pseudoatom, $k_1 = 10$ random positions in the simulation box are generated and one is selected with a probability $\exp(-\beta U_{1,i}^{ext})/\sum_j \exp(-\beta U_{1,j}^{ext})$, where $U_{1,j}^{ext}$ is the external energy of the CH_3 pseudoatom at the jth trial position interacting with the SWNT bundle and with the pseudoatoms of the other sorbate molecules. For each of the remaining five pseudoatoms ($m = 2, ..., 6$) of the hexane molecule, $k_m = 5$ trial positions are generated with a probability proportional to $\exp(-\beta U_{m,j}^{int})$. These positions are distributed on the surface of a sphere centered on the previously inserted pseudoatom of the molecule and whose radius is equal to the bond length. Each set of k_m trial orientations is generated by using the internal part of the potential $U_{m,j}^{int}$, whose probability depends on which type of pseudoatom is being inserted: for the second atom ($m = 2$) the internal potential energy is zero and as a result the trial positions are randomly distributed on a sphere, for the third atom ($m = 3$) the internal potential energy includes bond bending, and for the fourth and higher atoms ($m = 3, ..., 6$) the internal energy includes both bond bending and torsion. For each trial position j ($j = 1, ..., k_m$) the external energy $U_{m,j}^{ext}$ is calculated for interaction with the nanotube bundle, with the atoms of the other hexane molecules and with those atoms of the molecule already grown which are separated by more than four sites. From among the k_m trial positions, one is selected with a probability $\exp(-\beta U_{m,i}^{ext})/\sum_j \exp(-\beta U_{m,j}^{ext})$. During this growth process a bias is introduced and is removed by adjusting the acceptance rules.[32,33]

Note that because of the presence of nonbonded intramolecular interactions in the hexane force field, the imposed chemical potential in a configurational-bias GCMC simulation is shifted with respect to the true chemical potential by a temperature-dependent constant.[35] To calculate this shift we perform a separate simulation for one molecule in the ideal gas state; such an ideal gas simulation has to be performed only once at a given temperature.

Besides the usual trial step of molecule insertion/deletion, whose acceptance rate is enhanced by resorting to configurational-bias techniques, three additional types of Monte Carlo (MC) moves involving only individual molecules are necessary to sample the internal configuration of the simulation box: translation, rotation about the center-of-mass, and configurational-bias partial regrowth to change the internal conformation of the molecule.

Each run was equilibrated for (2×10^4)MC cycles followed by (3×10^4)MC cycles for the production period. Each cycle consists of $0.8N$ attempts to translate a randomly selected molecule, $0.2N$ trial rotations, $0.2N$ attempts to change the conformation of a molecule by using configurational-bias partial regrowth, and $\max\{20,0.2N\}$ molecule insertion/deletion steps. Here, N is the number of molecules in the simulation box at

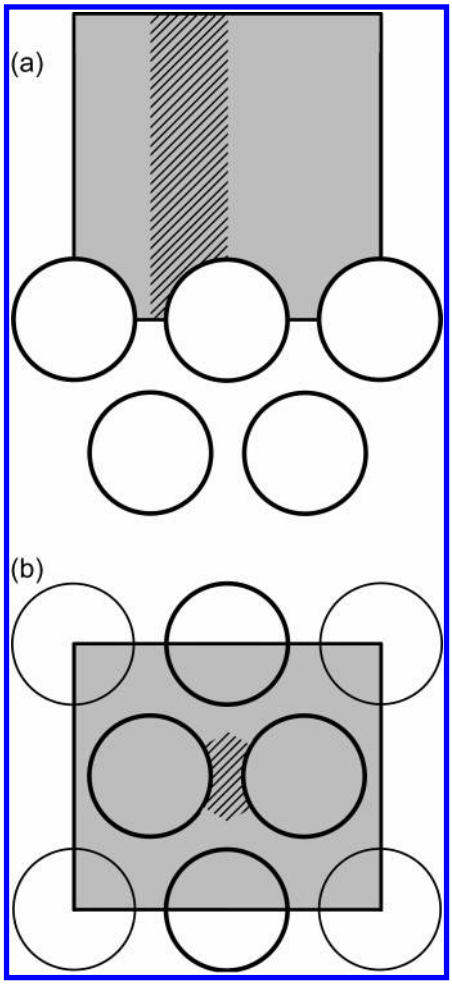

Figure 2. Cross section of the unit simulation box for GCMC study of hexane adsorption onto different adsorption sites of a bundle of open-ended SWNTs: (a) external groove sites and peripheral surface of the bundles and (b) internal and interstitial channels. A molecule located inside a nanotube of the bundle is under the interaction of the confining tube and its six nearest neighbors. The gray area represents the effective volume probed during the simulation. In each plot, the nanotubes printed in thicker lines are the contributing ones for the solid−fluid interaction potential of a pseudoatom of the adsorbate molecule placed in the hatched area.

the beginning of each cycle. The maximum displacement for translation and angle for rotation in the simulation box were adjusted during the equilibration phase to give a 50% acceptance rate. Standard deviations of the ensemble averages were computed by breaking the production run into five blocks.

The simulated temperatures are those of the adsorption experiments, but the simulated pressure range ($10^{-8} \leq P/P_0 \leq 0.9$) is much wider than that covered experimentally. Hexane adsorption was simulated on localized sites of homogeneous arrays of SWNTs for each diameter listed in Table 1, and conveniently combined into two major contributions to overall adsorption: (i) adsorption on the external surface of the bundles comprising grooves and peripheral surface (Figure 2a) and (ii) internal adsorption in endohedral and interstitial sites (Figure 2b).

Once the external and internal adsorption isotherms on homogeneous bundles were determined by simulation for each nanotube diameter, they were averaged over all nanotube diameters according to their weight fraction in the sample and combined into a total adsorption isotherm, $q_{sim}(P/P_0)$, which can be directly compared with experiment:

$$q_{sim}(P/P_0) = S_P\, q^{s}_{sim}(P/P_0) + \alpha(1-\eta) q^{i}_{sim}(P/P_0) \quad (4)$$

$$q^{\{s,i\}}_{sim}(P/P_0) = \sum_{D=\text{sample}} w_D q^{\{s,i\}}_{sim,D}(P/P_0) \quad (5)$$

In the above equations, $q^{s}_{sim,D}$ and $q^{i}_{sim,D}$ are respectively the simulated adsorption isotherms on the external surface and internal pore volume of a homogeneous bundle of nanotube diameter D, 100η is the wt % of impurities in the sample, and w_D is the weight fraction of nanotubes of diameter D (Table 1). It should be noted that $q^{i}_{sim,D}$ is calculated as the amount adsorbed per unit mass of the pure SWNT bundle, whereas $q^{s}_{sim,D}$ is computed as the amount adsorbed per unit external surface area of the purified bundle. S_P and α are structural parameters of the sample: S_P is its external surface area (m^2/g) and is obtained as the slope of the linear portion of the $q_{exp}(P/P_0)$ versus $q^{s}_{sim}(P/P_0)$ plot, where $q_{exp}(P/P_0)$is the experimental isotherm. Notice that the contribution of impurities is lumped into S_P as it should be discriminated only if one wants to determine unbiased values of other structural parameters of the bundle, such as average bundle diameter and average number of tubes per bundle. Detailed analysis of adsorption on nanotubes and impurities is presented in our related work.[36] α is the fraction of unblocked open-ended nanotubes in the sample and is determined by scaling $q^{i}_{sim}(P/P_0)$to yield a total isotherm $q_{sim}(P/P_0)$ that fits the experimental isotherm. Notice alternatively, it can be calculated as the ratio of experimental micropore volume to $(1-\eta)q^{i}_{sim}(P/P_0 \rightarrow 1)$. Notice that q^{i}_{sim} represents the theoretical upper limit on the internal adsorption isotherm, which is obtained after removing all impurities and opening all nanotubes. The values of S_P and α for samples EA95 and CVD80 are listed in Table 3, and have been previously determined by fitting eq 4 to the experimental N_2 adsorption isotherm at 77 K.[7] They are employed here to predict hexane adsorption on the same samples.

3. Results and Discussion

3.1. External Adsorption. Figure 3 shows simulated hexane adsorption isotherms, $q^{s}_{sim,D}(P/P_0)$, for the external surface of homogeneous SWNT bundles of tube diameter $D = 12.21$ Å. Inspection of snapshots of the simulation box (Figure 4) at very low pressures shows that external adsorption is localized in the grooves and does not spread to the peripheral surface of the bundles until $P/P_0 \approx 10^{-2}$. Perceptible adsorption (≥10% of adsorption at $P/P_0 \approx 0.9$) is observed only when P/P_0 is raised above this value, which validates the hypothesis made in the experimental study of organic adsorption on samples EA95 and CVD80,[28] where it is suggested that below $P/P_0 \approx 10^{-2}$ adsorption on samples with a significant fraction of open-ended nanotubes is mainly dominated by adsorption in the intratube space and not on the external surface of the bundles. Increasing the vapor concentration above $P/P_0 \approx 10^{-2}$ results in adsorption on the peripheral surface of the bundles, such that a complete monolayer is formed at $P/P_0 \approx 10^{-1}$ (Figure 4). Further increase in vapor concentration gives rise to multilayer adsorption until near saturation.

Notice that once the grooves are completely filled at about $P/P_0 \approx 10^{-2}$, the outer surface of the bundle loses its corrugation effect and the external adsorption isotherm becomes insensitive to nanotube diameter. The value of D influences the external adsorption isotherm only at very low relative pressures where adsorption is localized in the groove sites. However, the amounts adsorbed for that pressure region are negligible compared to the contribution from internal adsorption in the bundle when

TABLE 3: Structural Parameters for the Two SWNT Samples, Obtained by Fitting the Simulated and Experimental N_2 Adsorption at 77 K[a]

sample	S_P (m^2/g)	α
EA95	160	0.45
CVD80	437	0.60

[a] Agnihotri et al., ref 7.

the tubes are mostly opened. In agreement with a previous study,[7] one can thus state that for all practical purposes external adsorption is insensitive to nanotube diameter and consider the simulation data plotted in Figure 3 to be representative of all the nanotube sizes listed in Table 1. Note, however, that the specific external adsorption isotherm $S_P q^s_{sim}(P/P_0)$ (i.e., the amount adsorbed outside the bundles per unit mass of nanotubes) is much different for both samples, due to different values of S_P (Table 3).

The effect of temperature on adsorption in the external sites of the bundle is evident from the observed decrease of external loading when the temperature is raised from 298.15 to 323.15 K. This is typical for physisorption. However, it is also noticed that the change in external adsorption capacity due to temperature increase is more pronounced at lower vapor pressures, and as the gas-phase concentration increases the relative change becomes less noticeable. For example, increasing the temperature from 298.15 to 323.15 K results in 50% decrease in adsorption capacity at $P/P_0 \approx 10^{-4}$as opposed to 10% at $P/P_0 \approx 10^{-2}$ (Figure 3). This is because as the vapor concentration increases, multilayer adsorption starts to occur and the nanotubes have weaker interaction potential with the molecules adsorbed farthest from the bundle surface.

3.2. Internal Adsorption. Hexane adsorption in the internal sites of homogeneous SWNT bundles was simulated for each nanotube diameter listed in Table 1. The resulting adsorption isotherms, $q^i_{sim,D}(P/P_0)$, are plotted in Figure 5. It is observed that for $P/P_0 > 10^{-6}$ larger nanotubes have higher adsorption capacities than thinner nanotubes. This is to say that samples with large diameter SWNTs are more suitable adsorbents when the target organic vapor is present in concentrations exceeding 100's of ppbv. Samples of thin nanotubes, however, are desirable if adsorption of trace concentrations of organic vapors is required. Second, adsorption in all bundles steadily increases with increasing vapor concentration even when the gas-phase concentration is close to saturation. This behavior is different from N_2 adsorption in SWNT bundles at 77 K where the nanotubes are completely saturated at P/P_0 well below saturation ($P/P_0 = 10^{-6}$ for $D = 9$ Å and $P/P_0 = 10^{-3}$ for $D = 15.2$ Å).[7] It is believed that this difference between adsorption trends arises due to the fact that hexane is a larger, more complex molecule than nitrogen, which gives the former the advantage to reorient and, therefore, continue to pack with increasing pressure.

The effect of temperature on the internal adsorption isotherm is best depicted in Figure 5 for the two largest nanotubes (14 and 15.2 Å), which are the only ones for which the simulated relative pressure range covers conditions of low pore filling; the smaller nanotubes fill at relative pressures below the lowest value considered in this work. It is seen that the isotherm is shifted toward higher relative pressures with increasing temperature. At a fixed relative pressure, endohedral adsorption decreases with increasing temperature. For conditions close to complete pore filling, endohedral adsorption in a bundle remains almost unaffected by temperature, although a slight decrease of the saturation capacity is observed with increasing temperature, which is consistent with liquidlike behavior.

3.3. Total Adsorption. The total hexane adsorption isotherm for each sample was calculated by adding its external and internal adsorption contributions according to eq 4. The external surface area of the bundles (S_P) and scaling parameter for internal adsorption (α) were taken to be the same as those obtained previously[7] by applying a similar methodology to the experimental N_2 adsorption isotherm (Table 2). The total isotherms calculated for samples EA95 and CVD80 at 298.15, 310.15, and 323.15 K are plotted in Figure 6 along with the experimental isotherms.

It is seen that the simulated isotherms replicate the experimental isotherms of both samples for all tested temperatures (Figure 6). Such agreement demonstrates the versatility of the simulation procedure and the analytical techniques developed in our previous study.[7] Numerous observations can be made by comparing theoretical and experimental isotherms. First, internal adsorption dominates the total adsorption capacity of sample EA95 whereas external adsorption is more significant for sample CVD80; external adsorption on sample CVD80 is noticeable at lower P/P_0. This trend is because of differences in bundle morphology between the two samples. The existence of larger nanotubes in sample EA95 provides higher internal pore volume than the smaller nanotubes of sample CVD80. This fact, together with the S_P value being larger for sample CVD80 than for sample EA95, cause internal adsorption to dominate total adsorption of sample EA95 but the opposite for sample CVD80.

Second, at very low vapor concentrations ($10^{-8} < P/P_0 < 10^{-6}$ or 2 to 200 ppb) sample CVD80 has a higher organic vapor adsorption capacity than sample EA95 because small diameter nanotubes are filled at lower vapor concentrations (Figure 5). Due to limitations of our experimental setup this could not be observed experimentally.[28] It is, nevertheless, an important result as it reveals that the true potential of nanotubes as adsorbents for vapors at extremely low concentrations can be found in samples containing small diameter nanotubes. For bulk separation and gas storage, however, large nanotubes will be desirable.

Third, the effect of temperature on total adsorption capacity is apparent. The contribution from different adsorption sites to the observed decrease in adsorption with increasing temperature[28] cannot be determined experimentally, as gravimetric measurements are limited to determining total adsorption capacity only. By simulation, however, it is possible to calculate adsorption in different sites accurately enough to precisely determine the total adsorption capacity of a sample such that a near perfect replication of experimental data is obtained at all temperatures. Our analysis shows that the observed decrease in total adsorption is a result of significant lowering of adsorption on the peripheral surface of nanotube bundles in samples EA95 and CVD80, and a marginal decrease in endohedral adsorption (Figures 4 and 6). The effect of temperature on total adsorption capacity is more evident for sample CVD80 because external adsorption has a higher contribution for this sample. Therefore, it is reasonable to say that for most practical applications as temperature is raised, endohedral and groove sites are preferred over other adsorption sites (Figure 1).

3.4. Limiting Adsorption Capacity. From our analysis it is possible to calculate the limiting adsorption capacity of each sample for a hypothetical scenario of all nanotubes being opened and unblocked. This was performed by assuming $\alpha = 1$ and recalculating the total isotherm at 298.15 K. The resulting isotherms are shown in Figure 7. It is observed that opening all nanotubes causes at least a 2-fold increase in adsorption capacity of sample EA95 and a less significant increase for sample

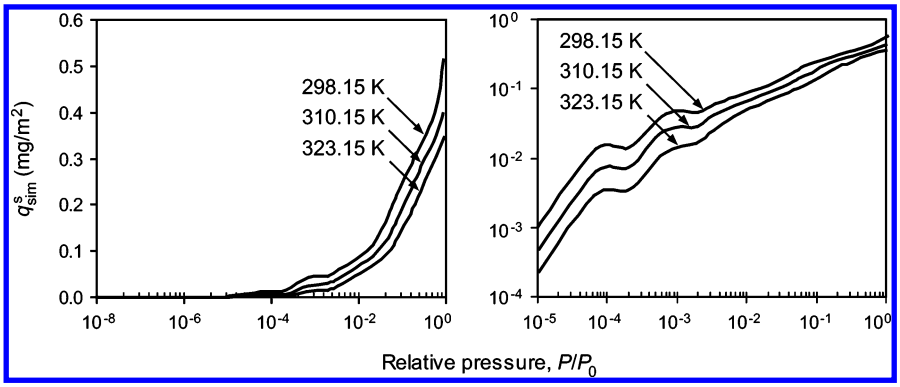

Figure 3. Effect of temperature on hexane adsorption on the peripheral surface of a homogeneous nanotube bundle comprising 12.21 Å SWNTs. Notice that significant adsorption is observed at $P/P_0 \geq 10^{-2}$ (left) and the effect of temperature is pronounced at lower vapor pressures (right).

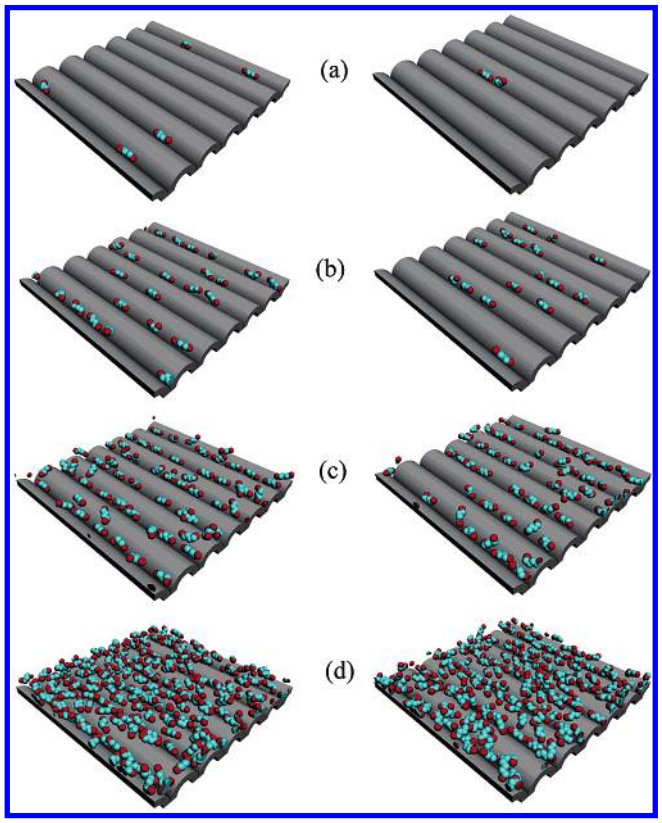

Figure 4. Snapshots of hexane adsorbed on the peripheral surface of a homogeneous nanotube bundle comprising 12.21 Å SWNTs at $T =$ 298.15 (left) and 323.15 K (right) at (a) $P/P_0 = 10^{-4}$, (b) 10^{-3}, (c) 10^{-2}, and (d) 10^{-1}. CH_3 and CH_2 pseudoatoms are shown in red and cyan, respectively.

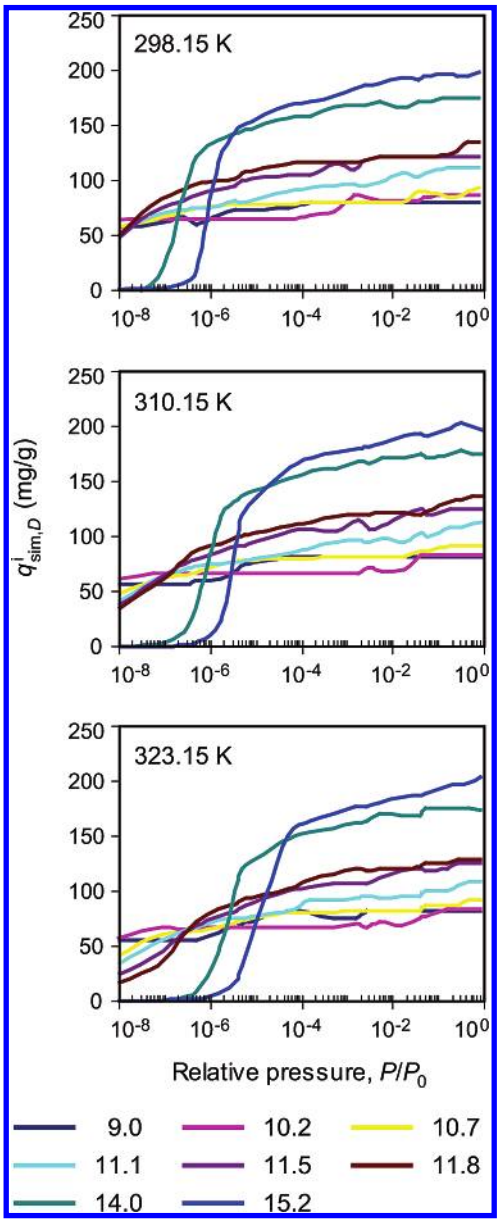

Figure 5. Simulated internal hexane adsorption isotherms for homogeneous bundles of SWNTs with diameters relevant to samples EA95 and CVD80 at (a) 298.15, (b) 310.15, and (c) 323.15 K. The lower horizontal legend lists the SWNT diameters in Å.

CVD80. Additionally, sample EA95 will have higher adsorption capacity for most P/P_0 values, except at very low ($P/P_0 \leq 10^{-6}$) and very high vapor concentration ($P/P_0 > 0.1$). Such a hypothetical scenario will be of valuable use when efficient analytical techniques to extract only open-ended nanotubes from as-grown materials are developed.

3.5. Adsorption of Other Organic Vapors. The simulated hexane adsorption isotherms were also compared with experimental isotherms previously obtained on the same samples for other organic compounds, such as toluene, methyl ethyl ketone (MEK), and cyclohexane.[28] The total organic adsorption is only 50% of the total pore volume.[28] This is because the interbundle distance (200 to 500 Å) is too wide to be completely utilized until saturation (i.e., $P/P_0 = 1.0$). This scenario is extremely difficult to measure experimentally, and calculate theoretically; therefore, organic adsorption is not fully able to use the mesoporosity of the sample. Simulations are able to reproduce the low-pressure experimental data of hexane, the subject molecule, but not toluene, MEK, and cyclohexane molecules.

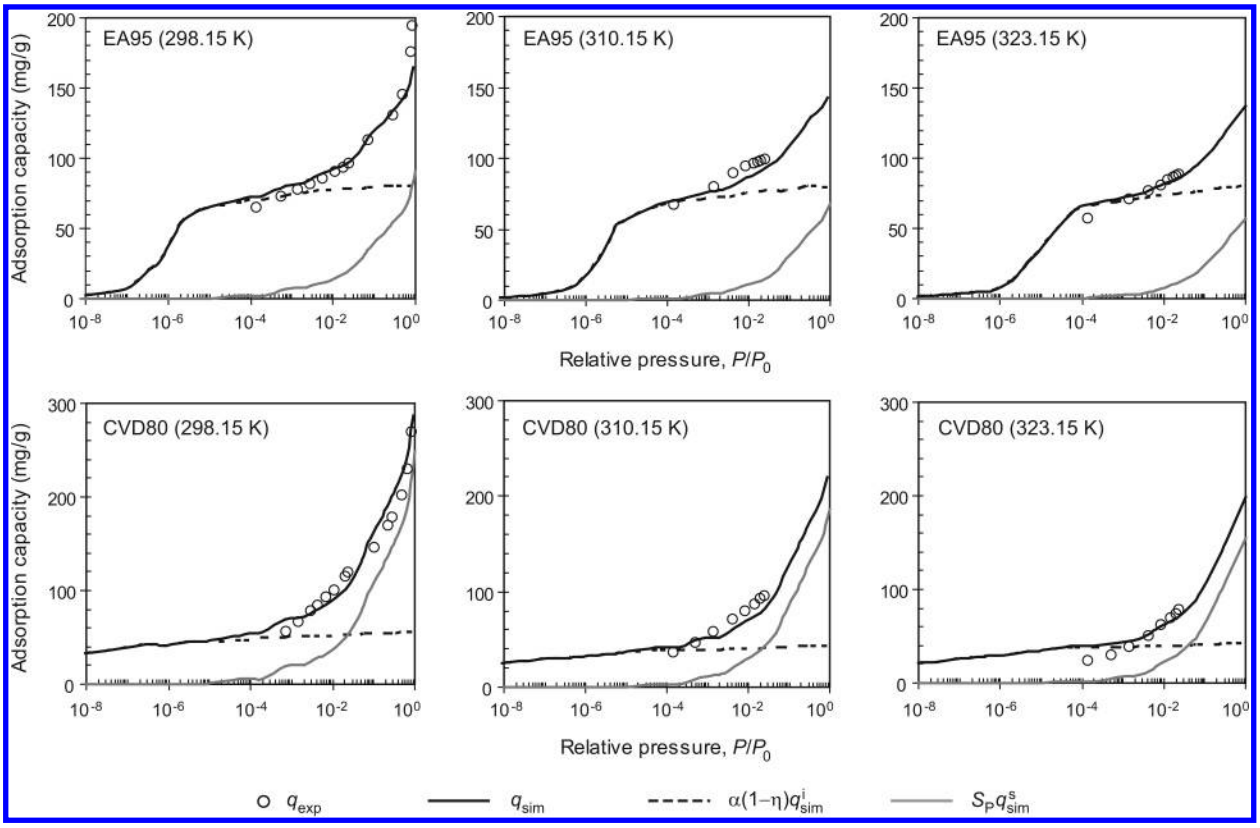

Figure 6. Simulated hexane adsorption isotherms at select temperatures for samples EA95 and CVD80. There is good agreement between the simulated data (lines) and the corresponding experiments (circles) for the two samples at all temperatures (R^2 for all plots >0.95). P_0 at 298.15, 310.15, and 323.15 K are 0.198, 0.323, and 0.53 atm, respectively.

There is some uncertainty in the measured adsorption data at very low pressure, which coupled to the magnification effects of bundle heterogeneity on adsorption at very low pressure, slightly deteriorates the agreement between experiments and simulation. However, as observed in Figure 8, there are no significant differences in experimental adsorption capacity between the various organic vapors to reach any conclusion regarding the dependence of total adsorption on specific molecular properties, such as dipole moment, shape, or size of a molecule. Therefore, it is very likely that adsorption trends explored by simulation for hexane are also applicable for most organic vapors, irrespective of differences in dipole moment, such as in MEK, and molecule shape, such as in toluene and cylcohexane. This is an important result, as it shows that the proposed methodology can be potentially applicable to more complex organic molecules with equal success.

4. Summary and Conclusions

Hexane adsorption on SWNT bundles has been studied both experimentally and by molecular simulation. The simulation procedure and analytical methods have been developed in our previous study to determine structural parameters of SWNTs, i.e, fraction of open-ended nanotubes and external surface area of nanotube bundles, in purified samples from the standard N_2 adsorption isotherm (77 K), which is commonly employed to determine BET surface area and pore volume. Here, we demonstrate that the same methodology can be applied to calculate adsorption of a more complex organic molecule. The total adsorption capacity is determined by summing the adsorption contribution from outside the bundles and that inside the bundles upon correcting the latter with the fraction of existing open-ended nanotubes. Theoretically calculated isotherms were

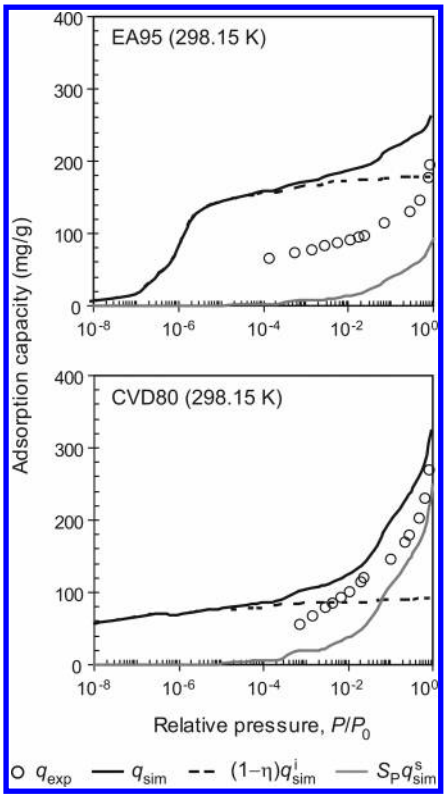

Figure 7. Limiting hexane adsorption on samples EA95 and CVD80 at 298.15 K. Total simulated capacities (solid lines) are much higher than experimental values (circles) for both samples, as internal adsorption has not been scaled for the fraction of open-ended nanotubes present in each sample.

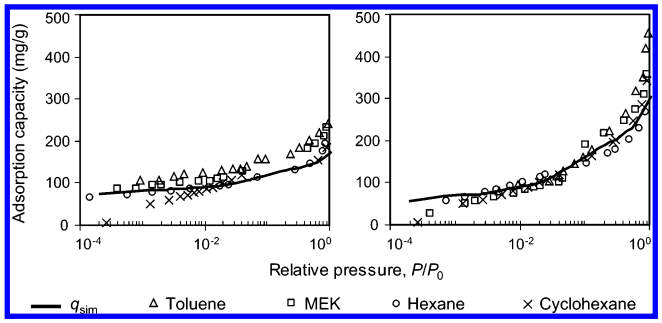

Figure 8. Comparison of simulated isotherms of hexane adsorption (lines) with experimental isotherms (symbols) for toluene, MEK, and cyclohexane vapors for samples EA95 (left) and CVD80 (right) at 298.15 K. $R^2 = 0.8$ to 0.95. P_0 values for toluene, MEK, and cyclohexane are 0.037, 0.118, and 0.128 atm, respectively.

compared with experimental data and a near perfect replication of experimental data is observed for the tested samples at all temperatures and relative vapor pressures. This demonstrates the versatility of our simulation procedure and the soundness of our methodology to characterize structural parameters relevant to adsorption in nanotubes.

The effect of temperature on adsorption was also studied, and it is found that adsorption inside nanotubes is strongly affected only at very low vapor concentrations ($P/P_0 \leq 10^{-6}$), and that the experimentally observed lowering of hexane adsorption capacity at higher temperatures is due mainly to decreased adsorption on the external surface of the bundles. Simulations can also be used to predict the adsorption isotherm for a hypothetical scenario in which all nanotubes in a sample are opened. This showed a 2-fold increase in the total adsorption capacity of one of the samples. Finally, it is found that simulated hexane adsorption isotherms follow the same trend as the experimental isotherms of other organic compounds, which shows that the adsorption mechanisms explored in this study are likely to be of general applicability to most organic vapors on SWNTs.

References and Notes

(1) Dresselhaus, M. S.; Dresselhaus, G.; Avouris, P. H. *Carbon nanotubes*: *synthesis*, *structure*, *properties and applications*; Topics in Applied Physics, No. 80; Springer: New York, 2000.

(2) Baughman, R. H.; Zakhidov, A. A.; Heer, W. A. Carbon nanotubes-the route toward applications. *Science* **2002**, *297*, 787.

(3) Talapatra, S.; Migone, A. D. Adsorption of methane on bundles of closed-ended single-wall carbon nanotubes. *Phys. Rev. B* **2002**, *65*, 045416.

(4) Du, W.; Wilson, L.; Ripmeester, J.; Dutrisac, R.; Simard, B.; Denommee, S. Investigation of the pore structure of as-prepared and purified HiPco single-walled carbon nanotubes by N_2/Ar adsorption-Implication for H_2 storage. *Nano Lett.* **2002**, *2*, 343.

(5) Shi, W.; Johnson, J. K. Gas adsorption on heterogeneous single-walled carbon nanotube bundles. *Phys. Rev. Lett.* **2003**, *91*, 015504.

(6) Agnihotri, S.; Rostam-Abadi, M.; Rood, M. J. Temporal changes in nitrogen adsorption properties of single-walled carbon nanotubes. *Carbon* **2004**, *42*, 2699.

(7) Agnihotri, S.; Mota, J. P. B.; Rostam-Abadi, M.; Rood, M. J. Structural characterization of single-walled carbon nanotube bundles by experiment and molecular simulation. *Langmuir* **2005**, *21*, 896.

(8) Fujiwara, A.; Ishji, K.; Suematsu, H.; Kataura, H.; Maniwa, Y.; Suzuki, S.; Achiba, Y. Gas adsorption in the inside and outside of single-walled carbon nanotubes. *Chem. Phys. Lett.* **2001**, *336*, 205.

(9) Matranga, C.; Bradley, B. Controlled confinement and release of gases in single-walled carbon nanotube bundles. *J. Phys. Chem. B* **2005**, *109*, 9209.

(10) Zhao, J.; Buldum, A.; Han, J.; Lu, J. P. Gas molecule adsorption in carbon nanotubes and nanotube bundles. *Nanotechnology* **2002**, *13*, 195.

(11) Chang, H.; Lee, J. D.; Lee, S. M.; Lee, Y. H. Adsorption of NH_3 and NO_2 molecules on carbon nanotubes. *Appl. Phys. Lett.* **2001**, *79*, 3863.

(12) Kong, J.; Franklin, N. R.; Zhou, C.; Chapline, M. G.; Peng, S.; Cho, K.; Dai, H. Nanotube molecular wires as chemical sensors. *Science* **2000**, *287*, 622.

(13) Varghese, O. K.; Kichambre, P. D.; Gong, D.; Ong, K. G. Gas sensing characteristics of multi-wall carbon nanotubes. *Sens. Actuators B* **2001**, *81*, 32.

(14) Yin, Y. F.; Mays, T.; McEnanaey, B. Adsorption of nitrogen in carbon nanotube arrays. *Langmuir* **1999**, *15*, 8714.

(15) Long, R. Q.; Yang, R. T. Carbon nanotubes as superior sorbents for nitrogen oxides. *Ind. Eng. Chem. Res.* **2001**, *40*, 4288.

(16) Gadd, G. E.; Blackford, M.; Moricca, S.; Webb, N. The world's smallest gas cylinders? *Science* **1997**, *277*, 933.

(17) Bourgrine, A.; Dupont-Pavlovsky, N.; Ghanbaja, J. Adsorption studies of a krypton film adsorbed on catalytically synthesized multiwalled carbon nanotubes: dependence on the nanotube morphology. *Surf. Sci.* **2002**, *506*, 137.

(18) Muris, M.; Dufau, N.; Bienfait, M.; Dupont-Povlovsky, N. Methane and krypton adsorption on single-walled carbon nanotubes. *Langmuir* **2000**, *16*, 7019.

(19) Mackie, E. B.; Wolfson, R. A.; Arnold, L. M.; Lafdi, K.; Migone, A. D. Adsorption studies of methane films on catalytic carbon nanotubes and on carbon filaments. *Langmuir* **1997**, *13*, 7197.

(20) Talapatra, S.; Zambano, A. Z; Weber, S. E.; Migone, A. D. Gases do not adsorb on the interstitial channels of closed-ended single-walled carbon nanotube bundles. *Phys. Rev. Lett.* **2000**, *85*, 138.

(21) Duren, T.; Keil, F. J. Molecular modeling of adsorption in carbon nanotubes. *Chem. Eng. Technol.* **2001**, *24*, 698.

(22) Mao. Z.; Lee, K. H.; Sinnott, S. B. Nanotubes as membranes: Predictions of atomistic simulations. *Energeia* **2003**, *14*, 1 (CAER, University of Kentucky).

(23) Eswaramoorthy, M.; Sen, R.; Rao, C. N. R. A study of micropores in single-wall carbon nanotubes by the adsorption of gases and vapors. *Chem. Phys. Lett.* **1999**, *304*, 207.

(24) Long, R. Q.; Yang, R. T. Carbon nanotubes as superior sorbents for dioxin removal. *J. Am. Chem. Soc.* **2001**, *123*, 2058.

(25) Bittner, E. W.; Smith, M. R.; Bockrath, B. C. Characterization of surfaces of single-walled carbon nanotubes using alcohols and hydrocarbons: a pulse adsorption technique. *Carbon* **2003**, *41*, 1231.

(26) Li, Q.; Yuan, D. Evaluation of multi-walled carbon nanotubes as gas chromatographic column packing. *J. Chromatogr. A* **2003**, *1003*, 203.

(27) Li, Q.; Yuan, D.; Lin, Q. Evaluation of multi-walled carbon nanotubes as an adsorbent for trapping volatile organic compounds from environmental samples. *J. Chromatogr. A* **2004**, *1026*, 283.

(28) Agnihotri, S.; Rood, M. J.; Rostam-Abadi, M. Adsorption equilibrium of organic vapors on single-walled carbon nanotubes. *Carbon* **2005**, *43*, 2379.

(29) Nikolaev, P.; Bronikowski, M. J.; Bradley, R. K.; Rohmund, F.; Colbert, D. T.; Smith, K. A.; Smalley, R. E. Gas-phased catalytic growth of single-walled carbon nanotubes from carbon monoxide. *Chem. Phys. Lett.* **1999**, *313*, 91.

(30) Bronikowski, M. J.; Willis, P. A.; Colbert, D. T.; Smith, K. A.; Smalley, R. E. Gas-phase production of carbon single-walled nanotubes from carbon monoxide via HiPco process: a parametric study. *J. Vacuum Sci. Technol. A* **2001**, *19*, 1800.

(31) Martin, G. M.; Siepmann, J. I. Transferable potentials for phase equilibria. 1. united-atom description of *n*-alkanes. *J. Phys. Chem. B* **1998**, *102*, 2569.

(32) Siepmann, J. I.; Frenkel, D. Configurational-bias Monte Carlo—a new sampling scheme for flexible chains. *Mol. Phys.* **1992**, *75*, 59.

(33) Frenkel, D.; Mooij, G. C. A. M.; Smit, B. Novel scheme to study structural and thermal properties of continuously deformable molecules. *J. Phys.: Condens. Matter* **1992**, *4*, 3053.

(34) de Pablo, J. J.; Laso, M.; Suter, U. W. Simulation of polyethylene above and below the melting point. *J. Chem. Phys.* **1992**, *96*, 2395.

(35) Smit, B. Grand canonical Monte Carlo simulations of chain molecules: adsorption isotherms of alkanes in zeolites. *Mol. Phys.* **1995**, *85*, 153.

(36) Agnihotri, S.; Mota, J. P. B.; Rostam-Abadi, M.; Rood, M. J. Adsorption site analysis of impurity embedded single-walled carbon nanotube bundles. *Carbon* **2006**. Accepted for publication.